Glycocalyx mechanotransduction mechanisms are involved in renal cancer metastasis

Heriberto Moran [a], Limary M. Cancel [a], Peigen Huang [b], Sylvie Roberge [b], Tuoye Xu [b], John M. Tarbell [a]* and Lance L. Munn [b]*

***a* - Wallace H. Coulter Laboratory,** *Department of Biomedical Engineering, The City College of New York, The City University of New York, New York, NY 10032, USA*

***b* - Edwin L. Steele Laboratories for Tumor Biology,** *Department of Radiation Oncology, Massachusetts General Hospital and Harvard Medical School, Charlestown, MA 02129, USA*

Correspondence to John M. Tarbell and Lance L. Munn: Department of Biomedical Engineering, The City College of New York, 160 Convent Ave, New York, NY 10031, USA. *limarycancel@yahoo.com (L.M. Cancel), jtarbell@ccny.cuny.edu (J.M. Tarbell), munn@steele.mgh.harvard.edu (L.L. Munn)*
https://doi.org/10.1016/j.mbplus.2021.100100

Abstract

Mammalian cells, including cancer cells, are covered by a surface layer containing cell bound proteoglycans, glycoproteins, associated glycosaminoglycans and bound proteins that is commonly referred to as the glycocalyx. Solid tumors also have a dynamic fluid microenvironment with elevated interstitial flow. In the present work we further investigate the hypothesis that interstitial flow is sensed by the tumor glycocalyx leading to activation of cell motility and metastasis. Using a highly metastatic renal carcinoma cell line (SN12L1) and its low metastatic counterpart (SN12C) we demonstrate in vitro that the small molecule Suberoylanilide Hydroxamic Acid (SAHA) inhibits the heparan sulfate synthesis enzyme N-deacetylase-N-sulfotransferase-1, reduces heparan sulfate in the glycocalyx and suppresses SN12L1 motility in response to interstitial flow. SN12L1 cells implanted in the kidney capsule of SCID mice formed large primary tumors and metastasized to distant organs, but when treated with SAHA metastases were not detected. In another set of experiments, the role of hyaluronic acid was investigated. Hyaluronan synthase 1, a critical enzyme in the synthetic pathway for hyaluronic acid, was knocked down in SN12L1 cells and in vitro experiments revealed inhibition of interstitial flow induced migration. Subsequently these cells were implanted in mouse kidneys and no distant metastases were detected. These findings suggest new therapeutic approaches to the treatment of kidney carcinoma metastasis.

Introduction

The incidence of kidney cancer has increased in the past 30 years, with about 76,080 new cases in 2021. More than 13,000 of these patients will die from the disease, and the five year survival rate for patients with metastatic disease is only 13% (cancer.org). Because the kidneys function as a filter to remove wastes from blood and maintain fluid and chemical homeostasis, renal cells are continuously exposed to dynamic fluid forces. The fluid dynamic environment is further exacerbated in tumors, where leaky blood vessels expose cancer cells to high levels of interstitial fluid flow [1]. Our previous work has suggested that these forces may enhance mechanobiological pathways to enhance cancer cell metastasis [2,3].

The surface of mammalian cells is coated with a layer of proteoglycans, glycoproteins, glycosaminoglycans (GAGs) and bound proteins

known as the glycocalyx [4,5]. The glycocalyx forms a mechanical interface with the cell microenvironment, and has been implicated in mechanotransduction, most notably in endothelial cells that line blood vessels [3–8]. Studies using vascular smooth muscle cells and fibroblasts demonstrated that interstitial flow through tissue matrix is also sensed by the glycocalyx, leading to enhanced cell migration [6]. Tumors have a dynamic microenvironment characterized by spatially and temporally heterogeneous interstitial flow caused by blood vessels that are highly permeable compared to normal vasculature [1,7,8]. This results in high interstitial fluid pressure and elevated interstitial flow velocities that may play a role in angiogenesis, lymphangiogenesis and fibroblast differentiation [8–11]. It has also been observed that high peritumoral interstitial flow velocity is associated with poor survival in humans with cervical carcinoma [12]. Several studies have demonstrated that metastatic cells increase their migration rates in response to flow [2,13,14]. In vitro studies that examined the effects of fluid flow on metastatic cells found that they can utilize flow-induced chemokine gradients to direct migration either away from or towards the main tumor mass [15,16]. Furthermore, several computational studies predict that bulky glycoproteins may enhance the clustering of integrins and other transmembrane proteins at adhesion sites, thus facilitating assembly of adhesion complexes and enhanced growth factor signaling – phenotypes associated with cancer [17–19].

The primary hypothesis of our work is that the glycocalyx is a mechanosenor for interstitial flow that activates cell motility and metastasis. In foundational work leading to the current study, we found that interstitial flow-induced shear stress can enhance the invasive potential of metastatic renal cancer cells. Exposing cells suspended in a 3-dimensional collagen matrix to interstitial flow in vitro, we showed that both short-term (1 or 4 h) and long-term (24 h) exposure to interstitial flow increased migration of highly metastatic SN12L1 cells but not low metastatic SN12C cells [2]. Furthermore, it has been shown that orthotopically implanted SN12L1 tumors are more invasive when compared to SN12C tumors [20]. Importantly, enzymatic removal of the GAG flow sensors, heparan sulfate (HS) or hyaluronic acid (HA) blocked interstitial flow- induced migration. Building on these in vitro observations, we genetically modified the highly metastatic SN12L1 cell line by knocking down the gene for N-Deacetylase N-Sulfotransferase 1 (NDST1), one of a family of four sulfotransferase enzymes in the synthetic pathway for HS [21]. Previous studies in vascular smooth muscle cells [22] and SN12L1 cells [3] showed that knockdown of NDST1 suppressed HS expression and strongly inhibited cell motility in response to interstitial flow in vitro. Metastasis was evaluated in vivo by injecting the parental or knockdown cells into the kidney capsules of SCID mice. Tumors formed from the NDST1 knockdown cells were characterized by a 95% reduction in metastasis compared to control cells with intact HS. There was also impairment in invasion to surrounding tissue in the knockdown animals [3].

In the present study, we had two main objectives: (1) To test a small molecule pharmaceutical that might produce the effects we observed by the genetic inhibition of NDST1 that greatly reduced metastasis. (2) To extend the in vitro observation that reduction of HA suppresses migration, to metastasis in vivo, by genetically modifying metastatic cells to reduce HA synthesis.

To address the first objective we used Suberoylanilide Hydroxamiccomple Acid (SAHA), a small molecule (264 Da) drug (Vorinostat) that, in addition to functioning as a histone deacetylase (HDAC) inhibitor [23], has been reported to inhibit the HS synthetic enzyme NDST1 in primary skin fibroblasts [24]. We hypothesized that SAHA can recapitulate the decreases in cell migration and metastasis we observed with the genetic suppression of HS [3]. We found that SAHA decreases NDST1 expression in SN12L1 cells in vitro and suppresses interstitial flow–induced migration of SN12L1 cells. Most significantly, it completely suppressed metastasis of SN12L1 cells in an orthotopic mouse model of renal carcinoma. To address the second objective, we genetically modified highly metastatic SN12L1 cells to knock down the gene for hyaluronan synthase 1 (HAS1), a critical enzyme in the synthetic pathway for HA [25]. We show that these cells have impaired response to interstitial flow in vitro and undetectable metastasis in the mouse model.

Results

SAHA treatment reduces NDST1 expression and flow-induced migration in vitro

To investigate whether SAHA could pharmacologically reduce the expression of NDST1, we performed a dose response study using SN12L1 cell lines treated with SAHA or DMSO (vehicle control). The results (Fig. 1) indicate that doses of 1.0 μM, 2.5 μM and 5.0 μM for 4 days dramatically reduce NDST1 at both the mRNA and protein levels.

Because the higher concentrations of SAHA (2.5 and 5.0 μM) decreased cell viability, we used 1.0 μM for further experiments. SN12L1 cells treated with 1.0 μm SAHA displayed suppression of flow-induced migration (Fig. 2), consistent with previous results where NDST1 knockdown in

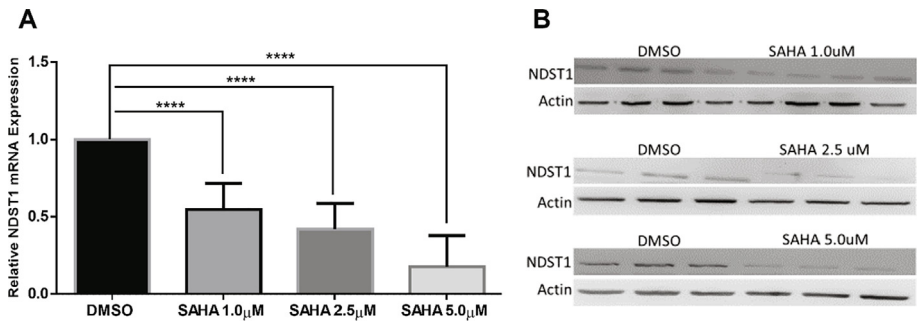

Fig. 1. Effect of treatment with SAHA on (A) relative NDST1 mRNA expression and (B) NDST1 protein levels. Cells were treated with 1.0, 2.5 and 5.0 μM SAHA, or DMSO (vehicle control) for 4 days. N = 9 for (A), n = 6 for (B). The data are represented as mean value ± SEM; ****p < 0.0001.

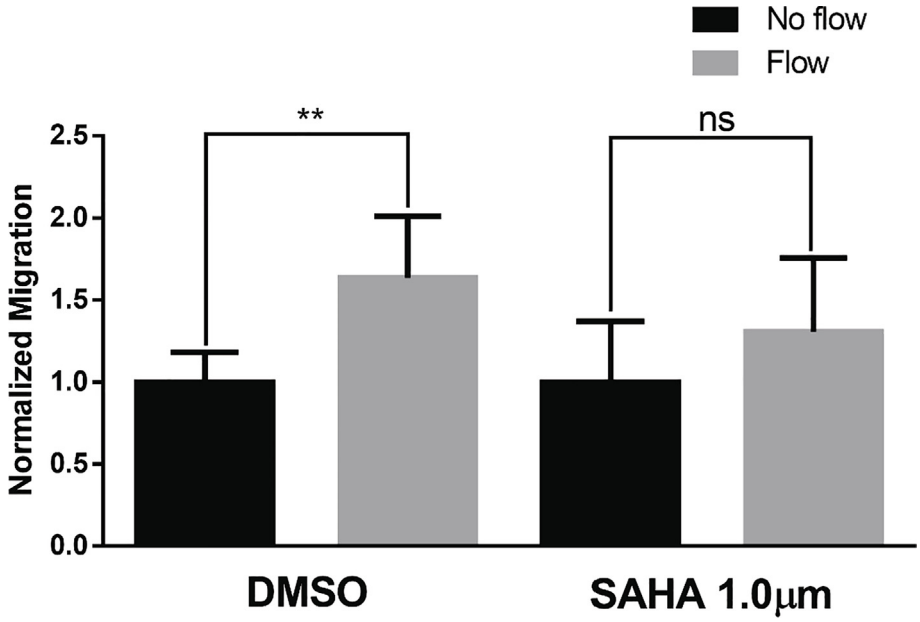

Fig. 2. Flow-induced migration in SN12L1 cells treated with DMSO (vehicle control) and 1.0 μM SAHA. Cells were treated for 4 days before being exposed to flow for 6 h. Results were normalized to no-flow controls. The data are represented as mean value ± SEM. N = 6; **p < 0.01, ns = not significant.

SN12L1 cells blocked flow-induced migration in vitro [3].

HAS1 deletion inhibits flow-induced migration in vitro

We next investigated the role of HA in the mechanotransduction of flow signals by knocking down HAS1, an enzyme involved in the synthesis of HA, using CRISPR/Cas9 (Fig. 3A). While there are other HAS enzymes (HAS2 and HAS3), HAS1 has been shown to be associated with cell migration and invasion in renal carcinoma cells [26]. The cells were subcloned by serial dilution in 96-well plates, and single colonies were subcultured. HAS1 mutant clones were identified by PCR, and a suitable knockout clone was evaluated for HAS1 protein expression by western blot (Fig. 3C). Decreased HA expression was confirmed by immunostaining with HA binding protein (HABP, Fig. 3B). To facilitate identification of metastatic cells in vivo, this clone was then transfected with a lentiviral vector containing mCherry targeted to the cell nucleus, and the cells were subcloned to obtain a pure mCherry/HAS1$^{-/-}$ knockout cell line (HAS1$^{-/-}$, Fig. 3D).

To determine whether HAS1 is involved in flow sensing, we performed flow-induced migration experiments in SN12L1 and HAS1$^{-/-}$ cell lines. We observed suppression of flow-induced migration in HAS1$^{-/-}$ cells in comparison to control cells (Fig. 4).

In previous work we showed that the hyaluronan receptor CD44 binds HA and provides a link to the

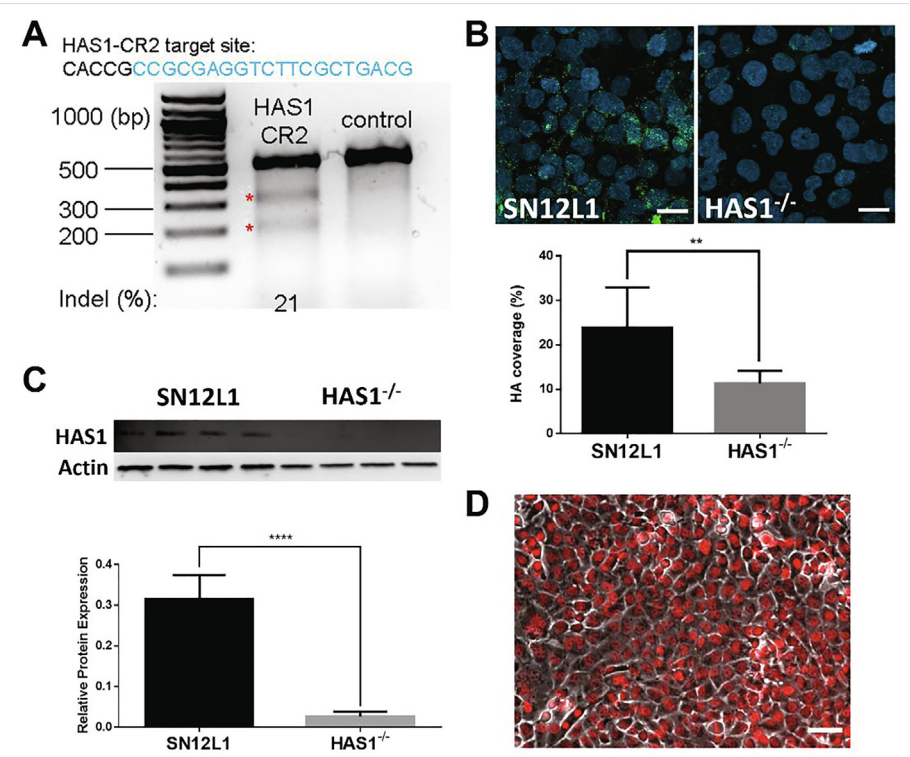

Fig. 3. Establishment of HAS1 knockout cell line by CRISPR. (A) T7EI assay shows 21% gene modification in cells transfected with HAS1-CR2; (B) top: representative images of HA binding protein immunostaining (green), cell nuclei were counterstained with DAPI (blue), bottom: intensity measurements of immunostaining for HABP show a significant decrease in coverage (n = 8, **p < 0.01); (C) top: western blot for HAS1, bottom: densitometry of western blots shows significant knockdown of protein expression (n = 4, p < 0.0001); (D) HAS1$^{-/-}$ after transfection with mCherry (red) targeted to cell nucleus, cell body shown in phase contrast. The data are presented as mean value ± SEM. Scale bars are 20 μm in (B), and 50 μm in (D). (For interpretation of the references to color in this figure legend, the reader is referred to the web version of this article.)

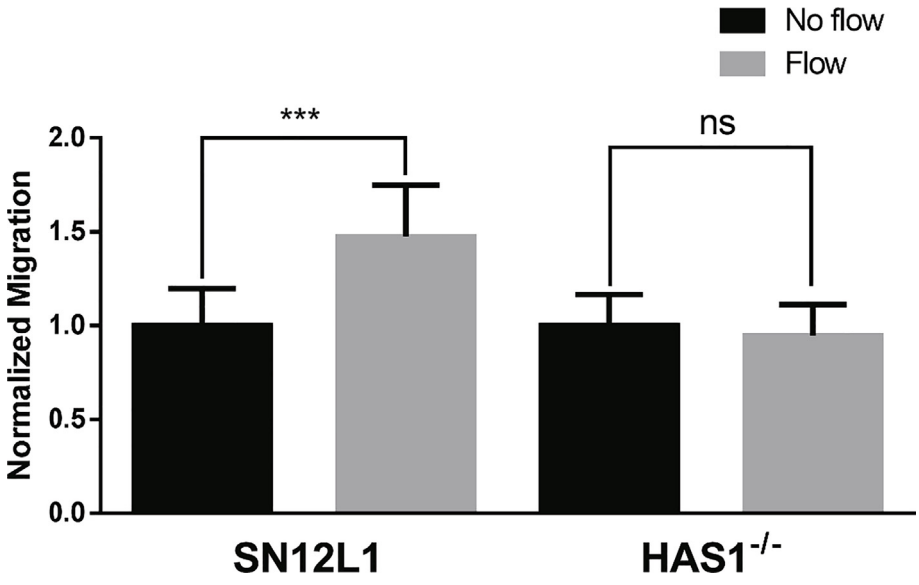

Fig. 4. Flow-induced migration response in of control SN12L1 cells and SN12L1 cells modified with CRISPR to reduce HAS1 expression (HAS1$^{-/-}$). Cells were exposed to flow for 6 h. Results were normalized to no-flow controls. The data are presented as mean value ± SEM. N = 6 for SN12L1, n = 9 for HAS1$^{-/-}$; ***p < 0.001, ns = not significant. The baseline migration (no-flow condition) in control and HAS1$^{-/-}$ was 78.5 ± 18 vs 87.0 ± 32, respectively; p = 0.445.

cell for mechanotransduction [2]. In the present work we discovered that Receptor for Hyaluronan Modulated Motility (RHAMM) also plays a role in flow induced mechanotransduction through HA. Supplementary data reveals that RHAMM knockdown blocks flow induced migration (Figs. S1–S3).

HAS1 knockdown and SAHA administration suppress renal carcinoma metastasis in an orthotopic mouse model

We next tested whether the reduction of HA on the cancer cell surface secondary to HAS1 deletion or administration of SAHA can decrease metastasis in a mouse model of renal carcinoma. Parental SN12L1 tumors were implanted under the kidney capsule of SCID mice and allowed to grow before being treated with SAHA or vehicle control. Treatment with the SAHA (40 μg/ml in drinking water) was started two weeks after tumor implantation. Because the SAHA needed to be dissolved in ethanol before mixing with water, we also included a group with 2% ethanol (EtOH) in the drinking water. After 30 days of primary tumor growth, the kidneys, along with the primary tumors, were resected and processed for histological analysis (Fig. 6). At this time, the tumors were ~120 mm^3 by caliper measurement. After another six weeks (to allow any seeded metastases to develop), we sacrificed the mice, performed necropsy and harvested the lungs, liver, contralateral kidney and spleen. In another group of mice, we implanted SN12L1 cells with HAS1 knocked down ($HAS1^{-/-}$). These were allowed to grow for 30 days and then removed with the kidney. After six weeks, they were sacrificed, and the organs were harvested, as previously described.

Analysis of the primary tumors showed no difference in tumor size or morphology (Fig. 5A). The tumor generally replaced most of the normal kidney, often producing a large fluid-filled structure within the kidney, resembling hydronephrosis (swelling of the kidney due to urine accumulation). This was likely due to blockage of the ureter by tumor growth. Primary tumors were observed in all the treatment groups, and no toxicity was observed due to $HAS1^{-/-}$ tumor growth or the SAHA or EtOH treatments.

Upon sacrifice and organ harvesting, metastases were evident in the untreated and EtOH control mice (Fig. 5B). Analyzing the endogenous fluorescence from the cancer cells, we detected many large metastatic colonies in the control and EtOH treated mice, but cancer cells were not detectable in the SAHA treated group, or in the mice implanted with $HAS1^{-/-}$ cells (Fig. 6). Automated image analysis confirmed this result (Fig. 7).

Discussion

This study further advances the hypothesis that interstitial flow shear stress is sensed by cancer cells through the glycocalyx, inducing cell motility and metastasis [12]. Tumor interstitial flow rates measured in vivo are elevated significantly depending on the tumor type [27,28]. In vitro models using a variety of cell lines have demonstrated that fluid

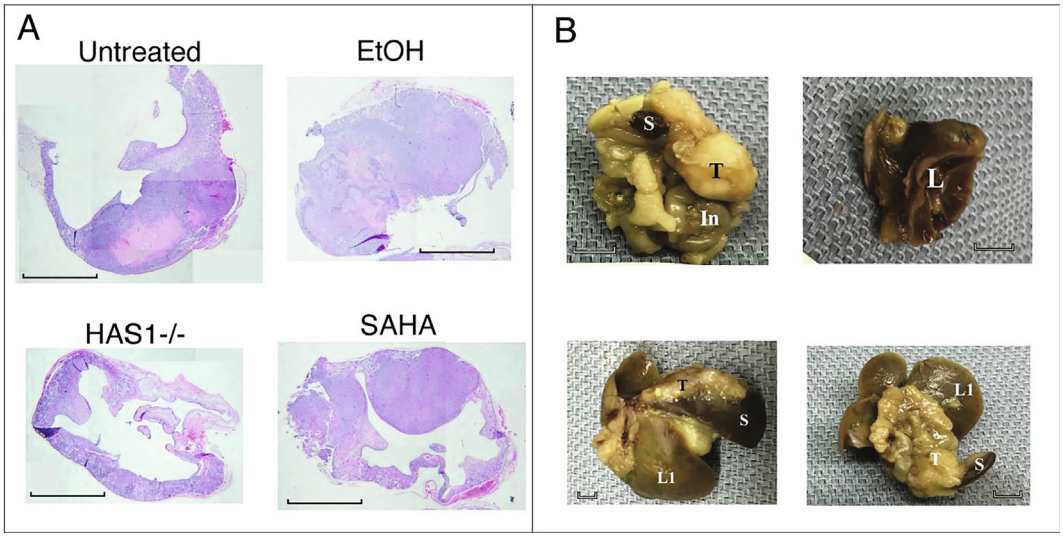

Fig. 5. Primary tumors and gross appearance of metastatic colonies. (A) Typical tumor-bearing kidneys resected from mice (H&E stain; total mice per group: untreated: 8; EtOH: 6; SAHA: 4; $HAS1^{-/-}$: 4). Mice implanted with $HAS1^{-/-}$ tumors or treated with vehicle control (2% EtOH) or SAHA had primary tumors that were similar in size and morphology to untreated mice. (B) Examples of metastatic colonization in the control mice. S: spleen; T: Tumor; L: Lung; L1: Liver; In: Intenstines. Scale Bars = 1 mm.

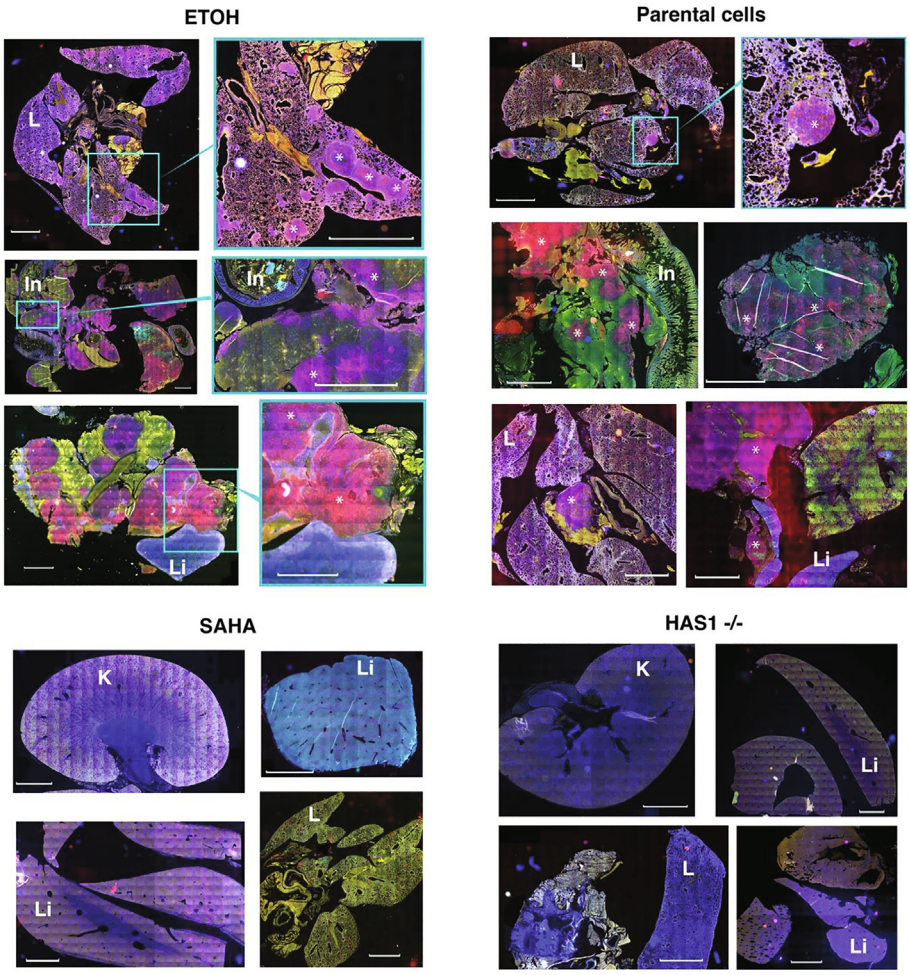

Fig. 6. Fluorescence imaging of histological sections in control and treated mice. Six weeks after primary tumor resection, mice were sacrificed and the organs were harvested. Vehicle control (EtOH) and untreated mice had metastatic colonies in multiple organs, while no metastases were detected in mice implanted with HAS1$^{-/-}$ cells or SAHA treated mice. The cancer cells are detected via the fluorescence of an intravital reporter, shown in red. Blue: dapi; green: tissue autofluorescence. L: Lung; Li: Liver; K: Kidney; In: Intestines. Scale bars: 0.5 mm. Asterisks highlight some of the metastatic colonies. (For interpretation of the references to color in this figure legend, the reader is referred to the web version of this article.)

shear stress associated with interstitial flow acts on tumor cells affecting focal adhesions, stromal cell recruitment, integrin expression, MMP expression and activation, and invasion rates [3,14,29]. In the present study we demonstrated that reduction of NDST1 and HS with the small molecule HDAC inhibitor SAHA blocked metastasis of highly metastatic renal carcinoma cells (SN12L1) in a mouse model.

While the reduction of NDST1 by SAHA in renal carcinoma cells is a novel finding and potentially important for mechanotransduction pathways, HDAC inhibitors can affect cell biology in multiple ways by changing the acetylation state of histones and modulating gene transcription [30]. Because of this, there has been much basic research and many clinical trials investigating the effects of SAHA on cancer cells and tumors. SAHA inhibits class I, II and IV HDACs and has been approved for treatment of T-cell lymphoma (brand name: Zolinza; Merck) [31,32]. In vitro, the combination of SAHA with mTOR inhibition decreases cancer cell proliferation, and treatment of subcutaneous renal carcinoma tumors in vivo inhibits growth [33]. However, this strategy showed limited efficacy in a phase I trial in advanced renal cell carcinoma patients [34]. In metastatic clear cell renal carcinoma, treatment with the combination of SAHA and bevacizumab (anti-vascular endothelial growth factor antibody) showed some efficacy in improving objective response rate and progression free survival [35]. The results of this trial suggest that blocking class II HDACs decreases hypoxia-inducible factor activity, thus synergizing with anti-VEGF treatment. Taken together, clinical data and our results show that HDAC inhibition is a potentially valid strategy to treat renal carcinoma, especially early in disease progression.

In addition to altering gene transcription by modifying acetylation status, there is evidence that

HDAC inhibitors like SAHA exert other effects in cells. For example, they can affect microtubule assembly and cell migration [36–38], which may be relevant for cancer metastasis. Furthermore, treatment with SAHA has the potential to decrease endothelial nitric oxide synthase (eNOS) expression [39]. eNOS is a major pathway affected by fluid shear stress and could therefore be associated with mechanotransduction in cancer cells. In previous work, we found that endothelial morphogenesis is HDAC1-dependent and that fluid flow increases the phosphorylation of HDAC1, its activity, and its export from the nucleus [11,38]. Furthermore, HDAC1 inhibition decreased endothelial morphogenesis and matrix metalloproteinase-14 expression. The present studies suggest that similar mechanisms may operate in renal carcinoma.

The GAGs HS and HA are believed to be the sensors of interstitial flow shearing forces. It is important to understand how the forces sensed by the GAGs are transmitted to the cell. In a previous in vitro study using the same kidney carcinoma cells, it was demonstrated that the HS proteoglycan core protein glypican 1, not syndecan 1, is the glycocalyx component that transmits the force to the cell where mechanotransduction proceeds [40]. This is consistent with a recent study of shear stress on endothelial cells that showed glypican 1 to be the mechanotransmitter mediating shear-induced nitric oxide production [41]. In [2] we showed that the cancer cell surface receptor for HA, CD44, is a transmitter of force sensed by HA to the cell. In supplement Figs. S1–S3 we provide evidence that the second major receptor for HA, RHAMM, is also involved in transmitting the force sensed by HA. In another study it has been noted that extracellular RHAMM-CD44 partnering sustains CD44 surface display and enhances CD44-mediated signaling through ERK1/2 [42]. This supports a recent study of chondrosarcoma cell lines that reported interstitial flow and fluid shear stress induced MMP-7 expression and enhanced invasion via an ERK1/2 signaling pathway [43], and the earlier study by Qazi et al. [2] that showed suppression of flow induced migration by an MMP inhibitor. The interplay between these two receptors in mediating metastasis has not been addressed in the current study. Cell invasion may also be enhanced by other effects of interstitial flow on cells including matrix tethering, cytoskeletal polymerization, enhanced integrin expression, enhanced normal stresses, and focal adhesion formation, as well as glycocalyx mediated mechanotransduction [14]. Further investigation into the role of these mechanisms in putative interstitial flow induced metastasis will be important for the development of therapeutics to suppress metastasis.

Our study has some notable limitations. Although the in vitro results of the present study suggest that the differences in metastasis between control cells and cells with reduced HS or HA are the result of altered flow mechanosensing in the cells with diminished glycocalyx, interstitial flow could not be precisely controlled in the animal studies over the long course of the experiments due to the lack of current methodologies for monitoring or controlling interstitial flow noninvasively. Future studies should address whether mechanisms such as growth factor presentation, receptor clustering, or as we suggest, mechanotransduction, is the primary function of cancer cell surface HS and HA in metastasis in vivo. In addition, we found that reduction of tumor cell HA through HAS1 knockdown can suppress metastasis in an orthotopic model of renal carcinoma (Figs. 6 and 7). We did not consider other HAS enzymes that might be effective, and we have not measured the concentrations of glycosidase and hyaluronidase enzymes that might degrade HA in our experiments. However, our data show that the parental cells have significant HA on their surface, suggesting that any enzymes produced by the cells are leaving abundant HA on the cell surface (Fig. 3B), whereas the HAS1 knockdown cells have significantly less HA. In addition, other studies of metastatic renal carcinoma cells have revealed an abundance of the HA receptors CD44 and RHAMM on the cells suggesting a significant presence of HA on their surfaces [2,44]. Finally, while inhibition of HA or NDST1 seems to be effective in our animal model, we did not pursue reduction of other HS synthetic enzymes that might also be effective.

Taken together, previous work and the current results suggest the mechanisms for flow-induced invasion and metastasis summarized in Fig. 8. Mechanical deformation of cell-surface GAGs including HA and HS transduce signals through heparan sulfate proteoglycans – glypicans, syndecans [4,5,40], and HA receptors – CD44 and RHAMM. HDACs can enhance HS expression through NDST1, facilitating the mechanotransduction, and RHAMM associated with CD44 is likely involved in the upstream response [42]. In addition to regulation of NDST1, HDACs are involved in modulation of multiple programs associated with cell migration and MMP expression [45]. In the present study, we have shown that interfering with HA production, HS synthesis (through NDST1) or HDAC activity can inhibit cell migration and metastasis. These results suggest that therapies targeting HA, HDACs or NDST1 should have efficacy in limiting the progression and metastasis of renal carcinoma.

Methods

Cell culture

All chemicals were from Millipore Sigma (St. Louis, MO) unless otherwise noted. Low (SN12C) and high (SN12L1) metastatic human renal carcinoma cell lines were obtained courtesy of Dr. Isaiah Fidler, MD Anderson Cancer Center.

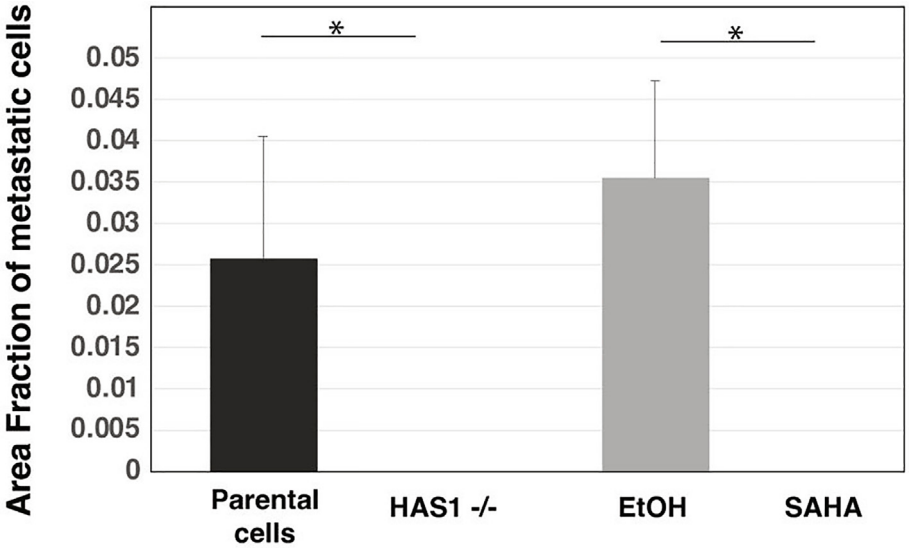

Fig. 7. Inhibition of metastasis in mice bearing SN12L1 HAS1$^{-/-}$ tumors and in mice bearing SN12L1 tumors treated with SAHA. Six weeks after primary tumor resection, mice were sacrificed, and the organs were harvested. Vehicle control (EtOH; n = 6) and untreated mice (n = 8) had metastatic colonies in multiple organs, while no metastases were detected in mice implanted with HAS1$^{-/-}$ cells (n = 4; *p < 0.05) or SAHA treated mice (n = 4; *p < 0.05).

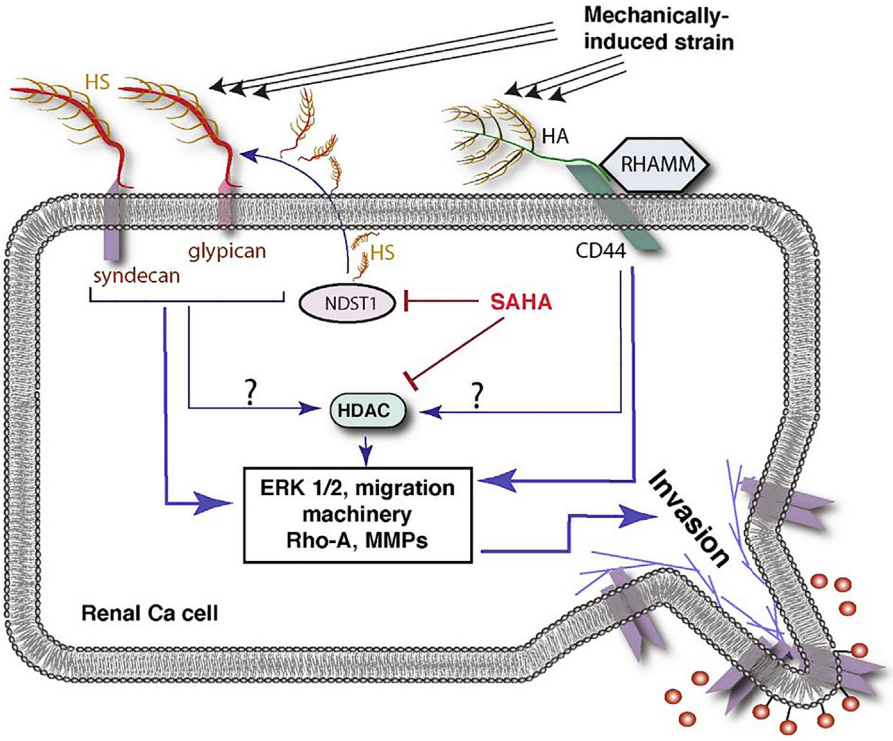

Fig. 8. Putative mechanisms of flow-induced renal carcinoma invasion and metastasis.

Following MD Anderson protocols [46], cells were cultured in minimum essential medium (MEM) supplemented with 10% fetal bovine serum (Atlanta Biologicals, Flowery Branch, GA), 1% penicillin/streptomycin, 1% L-glutamine, 2× Vitamin solution, 1× non-essential amino acids solution, and 1 mM sodium pyruvate. Cultures were kept at 37 °C, 5% CO_2.

Protein quantification

Cell lysis: Cells were rinsed 3 times in cold phosphate buffered saline (PBS) and lysed in RIPA buffer containing 0.1 mL Halt protease inhibitor cocktail (Thermo Scientific, Rockford, IL) and 0.1 mL Halt phosphatase inhibitor cocktail I (Roche, Basel, Switzerland). Cells were then scraped and sonicated 3 times for 10 s.

Western immuno-blotting: Cell extracts were suspended in 2× Laemmli sample buffer (Bio-Rad, Hercules, CA) and separated by 12% SDS-PAGE. Proteins were electrophoretically transferred to PVDF membranes. Membranes were blocked in 5% nonfat dry milk at room temperature for 1 hr before incubation in the appropriate dilution of primary antibodies against RHAMM, (1:500; Abcam), NDST1 (1:1000; Proteintech), and β-Actin (1:5000; ThermoScientific, Rockford, IL) in 5% nonfat dry milk and 0.1% Tween-20 overnight at 4 °C. Blots were washed three times for 15 min, followed by incubation in HRP-conjugated secondary antibody in 5% nonfat dry milk and 0.1% Tween-20 for 1hr at room temperature. Visualization of bands was achieved using the ECL kit (Thermo Scientific, Rockford, IL). Protein bands were detected with the ChemiDoc XRS system with Quantity One software (Bio-Rad; Hercules, CA), and quantified by densitometry using ImageJ.

siRNA transfection

siRNA oligonucleotides were purchased from Integrated DNA Technologies (Skokie, IL). SN12L1 cells were seeded at a density of 2.4×10^6 cells in six-well plates, grown for 24 h, and transfected with siRNA oligos targeting RHAMM (siRHAMM) using Lipofectamine RNAiMAX (ThermoFisher, Waltham, MA) according to the manufacturer's instructions. As a negative control, cells were transfected with scrambled RNA oligos. siRHAMM oligos were: 5′-GUCAAGAAUCAUGGAAGUAAACATC3′ and 3′CACAGUUCUUAGUACCUUCAUUUGUAG-5′.

RNA quantification

Total RNA was extracted using the RNeasy Mini kit (Qiagen, Hilden, Germany) and immediately treated with DNase I (New England BioLabs, Ipswich, MA) to remove possible DNA contamination. 1 μg of RNA was reverse transcribed to cDNA using the High-Capacity cDNA Reverse Transcription kit (ThermoFisher, Waltham, MA). Quantitative real time RT-PCR was performed on the 7000 Real Time PCR System (Applied Biosystems, Foster City, CA). The primers used were the following: RHAMM Forward-5′-tgg aag caa ggc taa atg ct-3′ and Reverse-5′-acc tgc agc ttc atc tcc at-3′, NDST1 Forward-5′- atg gca tca tgg ttc tcc ca-3′ and Reverse-5′-gcc agg gta ctc gtt gta ga-3′, β-Actin Forward-5′-cct gac ctg ccg tct aga aa-3′ and Reverse-5′-tta ctc ctt gga ggc cat gt-3′.

Cell migration assay

For the migration assay, 50,000 SN12L1 or SN12C cells were suspended in 2 mg/ml type I collagen and immediately incubated in type I collagen pre-coated culture inserts (8 μm pores) in 12-well plates. The Cell/collagen suspension inserts were incubated for 16 h with 800 μl of serum-containing MEM media to allow cell spreading. The collagen gels containing SN12L1, SN12C, or modified cells were exposed to 10 min of interstitial flow to compact the gels. No-flow control gels were placed in the incubator while flow gels were exposed to 6 h of interstitial fluid flow as previously described [2,14]. After flow, the migration assay was performed by incubating the suspensions with 1 nM TFG-α in the companion well for 48 h of migration (without flow). At the end of the migration assay, cells that migrated to the underside of the filter were fixed and stained using Diff-Quick (Siemens, Munich, Germany). Cells were visualized and counted as a quantitative measure of invasion using a bright field microscope. These methods have been described in great detail in Qazi et al. [2,14].

SAHA treatment in cell cultures

SN12L1 cells were treated with SAHA 1 μM, 2.5 μM, or 5 μM for 4 days. For migration assays, SN12L1 cells were treated with 1 μM SAHA for 4 days prior to static or flow conditions. The SAHA concentration was maintained throughout the flow period. Controls were treated with appropriate concentrations of DMSO.

Establishment of HAS1 knockout cell line

To establish a HAS1 knockout cell line, we randomly chose three guide RNA (gRNA) sequences from GeCKOv2 Human Library (http://genomeengineering.org/gecko/?page_id=15) targeting HAS1 gene. The gRNA sequences were cloned into the pX330 vector (http://www.addgene.org/42230/) containing Cas9. The plasmids were transfected into the SN12L1 cells using Lipofectamine 3000 (Invitrogen). Genomic DNA was isolated using the DNeasy Blood & Tissue kit (Qiagen, Hilden, Germany) and targeting efficiency was evaluated by T7 endonuclease I assay (T7EI; New England Biolabs). The target sequence for HAS1-CR2 was CACCGCCGCGAGGTCTTCGCTGACG. Primers for T7EI assay were HAS1-forward TCTGTACATTGAAGGAAAGACC and HAS1-reverse GCAGTGTGGCGCTGA. PCR was performed in a thermal cycler (Biorad, Hercules, CA), the products run on a 1.5% agarose gel, and

imaged in the ChemiDoc XRS system with Quantity One software (Bio-Rad, Hercules, CA).

Immunofluorescence staining and quantification of HA

SN12L1 and HAS1$^{-/-}$ cells were immunostained for HABP as previously described [47]. Briefly, cells were fixed with 2% paraformaldehyde/0.1% glutaraldehyde for 30 min at room temperature and blocked with 2% goat serum for 30 min. Cells were then incubated overnight at 4 °C with biotinylated HABP. After washing 3× in PBS, cells were incubated with Alexa Fluor 488 anti-Biotin (Jackson ImmunoResearch Lab, West Grove, PA) and counterstained with DAPI. Cells were imaged with a Zeiss LSM 800 laser scanning microscope. HA coverage was determined using ImageJ software, as previously described [47].

Mouse metastasis model

All animal protocols were approved by the Institutional Animal Care and Use Committee (IACUC) of the Massachusetts General Hospital (protocol #2004N000091). All experiments were performed in accordance with relevant guidelines and regulations, and reporting follows the recommendations in the ARRIVE guidelines.

HAS1$^{-/-}$ model: SN12L1 HAS1$^{-/-}$ cells were transfected with the intravital reporter mCherry to facilitate identification of metastatic cells. One million SN12L1 or SN12L1 HAS1$^{-/-}$ mCherry cells were implanted under the left kidney capsule of SCID mice. Primary tumors were allowed to grow for 30 days, and then the left kidneys, with the primary tumors, were removed. After six weeks more days, the mice were sacrificed, and organs were harvested for analysis of metastases.

SAHA treatment: SN12L1 cells were infected with Orange viral particles (pWPXL-Orange, gift from Dr. Danwei Huangfu) to facilitate identification of metastatic cells. One million cells were implanted under the left kidney capsule of SCID mice. Primary tumors were allowed to grow for two weeks, and then treatment was started. Groups were 1) untreated, 2) 2% ethanol in drinking water and 3) treatment with SAHA (dissolved in ethanol and added to drinking water; final concentration = 40 μg/ml). On day 30 after tumor implantation, the left kidney and primary tumor were resected and processed for histological analysis. After another six weeks (to allow any seeded metastases to develop), we sacrificed the mice, performed necropsy and harvested the lungs, liver, contralateral kidney and spleen.

Tissue processing and image analysis

The harvested tissues were embedded in OCT medium and sectioned to the center of the tissue. Then 200 μm (thick) sections were collected and stained with Dapi for fluorescence microscopy. The sections were scanned using a Zeiss Axioscan slide scanner to collect three color channels and the CZI were opened and analyzed using FIJI image analysis software (https://imagej.net/software/fiji/).

The raw CZI files were converted to 8-bit TIF files and the auto contrast command adjusted the image contrast of all three channels. The Dapi channel was segmented using the auto segment function, and then was subjected to a series of binary dilations and erosions to enlarge the nuclei so the resulting image approximated the total tissue area. This image was then measured and the number of positive pixels was recorded and used as an estimate of the total tissue area. The red channel was manually thresholded to create the binary image, and then this image was measured to record the number of cancer cell pixels in the image. The ratio of cancer to total pixels was calculated and compared between groups.

Data analysis

GraphPad Prism was used to perform statistical analysis. Results are presented as mean ± SEM and differences were considered significant when $p < 0.05$. When comparing two groups, statistical analyses were performed using unpaired two-tailed student's *t*-test.

DECLARATION OF COMPETING INTEREST

The authors declare the following financial interests/personal relationships which may be considered as potential competing interests: Lance L Munn owns equity in Bayer AG and is a consultant for SimBiosys. Neither any reagent nor any funding from these organizations was used in this study.

Acknowledgements

Research supported by NIH Grant RO1CA204949.

Authors Contributions

HM, JMT, and LLM designed the research; HM, LMC, PH, SR, and TX performed the research and analyzed data; HM, LMC, JMT, and LLM

wrote the manuscript. All authors read and approved the final manuscript.

Appendix A. Supplementary data

Supplementary data to this article can be found online at https://doi.org/10.1016/j.mbplus.2021.100100.

Received 4 October 2021;
Accepted 31 December 2021;
Available online 6 January 2022

Keywords:
Glycocalyx;
Metastasis;
Mechanotransduction;
Renal carcinoma

Abbreviations:
GAG, Glycosaminoglycan; HS, Heparan Sulfate; HA, Hyaluronic Acid; NDST1, N-Deacetylase N-Sulfotransferase 1; SAHA, Suberoylanilide Hydroxamic Acid; HDAC, Histone Deacetylase; HAS1, Hyaluronan Synthase 1; HABP, Hyaluronic Acid Binding Protein; RHAMM, Receptor for Hyaluronan Modulated Motility; $HAS1^{-/-}$, HAS1 knockout cell line; eNOS, Endothelial Nitric Oxide Synthase

References

[1] Nia, H.T., Munn, L.L., Jain, R.K., (2020). Physical traits of cancer. *Science*, **370** (6516)
[2] Qazi, H., Palomino, R., Shi, Z.D., Munn, L.L., Tarbell, J.M., (2013). Cancer cell glycocalyx mediates mechanotransduction and flow-regulated invasion. *Integr. Biol. (Camb.)*, **5** (11), 1334–1343.
[3] Qazi, H., Shi, Z.D., Song, J.W., Cancel, L.M., Huang, P., Zeng, Y., Roberge, S., Munn, L.L., Tarbell, J.M., (2016). Heparan sulfate proteoglycans mediate renal carcinoma metastasis. *Int. J. Cancer*, **139** (12), 2791–2801.
[4] Iozzo, R.V., Sanderson, R.D., (2011). Proteoglycans in cancer biology, tumour microenvironment and angiogenesis. *J. Cell Mol. Med.*, **15** (5), 1013–1031.
[5] Teng, Y.-F., Aquino, R.S., Park, P.W., (2012). Molecular functions of syndecan-1 in disease. *Matrix Biol.*, **31** (1), 3–16.
[6] Shi, Z.-D., Ji, X.-Y., Qazi, H., Tarbell, J.M., (2009). Interstitial flow promotes vascular fibroblast, myofibroblast, and smooth muscle cell motility in 3-D collagen I via upregulation of MMP-1. *Am. J. Physiol. Heart Circ. Physiol.*, **297** (4), H1225–H1234.
[7] Goel, S., Duda, D.G., Xu, L., Munn, L.L., Boucher, Y., Fukumura, D., Jain, R.K., (2011). Normalization of the vasculature for treatment of cancer and other diseases. *Physiol. Rev.*, **91** (3), 1071–1121.
[8] Jain, R.K., Tong, R.T., Munn, L.L., (2007). Effect of vascular normalization by antiangiogenic therapy on interstitial hypertension, peritumor edema, and lymphatic metastasis: insights from a mathematical model. *Cancer Res.*, **67** (6), 2729–2735.
[9] Ng, C.P., Swartz, M.A., (2003). Fibroblast alignment under interstitial fluid flow using a novel 3-D tissue culture model. *Am. J. Physiol. Heart Circ. Physiol.*, **284** (5), H1771–H1777.
[10] Rutkowski, J.M., Boardman, K.C., Swartz, M.A., (2006). Characterization of lymphangiogenesis in a model of adult skin regeneration. *Am. J. Physiol. Heart Circ. Physiol.*, **291** (3), H1402–H1410.
[11] Song, J.W., Daubriac, J., Tse, J.M., Bazou, D., Munn, L.L., (2012). RhoA mediates flow-induced endothelial sprouting in a 3-D tissue analogue of angiogenesis. *Lab Chip*, **12** (23), 5000–5006.
[12] Hompland, T., Lund, K.V., Ellingsen, C., Kristensen, G.B., Rofstad, E.K., (2014). Peritumoral interstitial fluid flow velocity predicts survival in cervical carcinoma. *Radiother. Oncol.*, **113** (1), 132–138.
[13] Shieh, A.C., Rozansky, H.A., Hinz, B., Swartz, M.A., (2011). Tumor cell invasion is promoted by interstitial flow-induced matrix priming by stromal fibroblasts. *Cancer Res.*, **71** (3), 790–800.
[14] Qazi, H., Shi, Z.-D., Tarbell, J.M., Deb, S., (2011). Fluid shear stress regulates the invasive potential of glioma cells via modulation of migratory activity and matrix metalloproteinase expression. *PLoS ONE*, **6** (5), e20348.
[15] Polacheck, W.J., Charest, J.L., Kamm, R.D., (2011). Interstitial flow influences direction of tumor cell migration through competing mechanisms. *Proc. Natl. Acad. Sci. U. S. A.*, **108** (27), 11115–11120.
[16] Shields, J.D., Fleury, M.E., Yong, C., Tomei, A.A., Randolph, G.J., Swartz, M.A., (2007). Autologous chemotaxis as a mechanism of tumor cell homing to lymphatics via interstitial flow and autocrine CCR7 signaling. *Cancer Cell*, **11** (6), 526–538.
[17] Desgrosellier, J.S., Cheresh, D.A., (2010). Integrins in cancer: biological implications and therapeutic opportunities. *Nat. Rev. Cancer*, **10** (1), 9–22.
[18] Paszek, M.J., Boettiger, D., Weaver, V.M., Hammer, D.A., Lauffenberger, D., (2009). Integrin clustering is driven by mechanical resistance from the glycocalyx and the substrate. *PLoS Comput. Biol.*, **5** (12), e1000604.
[19] Shibue, T., Weinberg, R.A., (2009). Integrin beta1-focal adhesion kinase signaling directs the proliferation of metastatic cancer cells disseminated in the lungs. *Proc. Natl. Acad. Sci. U. S. A.*, **106** (25), 10290–10295.
[20] Bockhorn, M., Roberge, S., Sousa, C., Jain, R.K., Munn, L.L., (2004). Differential gene expression in metastasizing cells shed from kidney tumors. *Cancer Res.*, **64** (7), 2469–2473.
[21] Varki, A., Cummings, R.D., Esko, J.D., Stanley, P., Hart, G.W., Aebi, M., Darvill, A.G., Kinoshita, T., Packer, N.H., Prestegard, J.H., Schnaar, R.L., Seeberger, P.H., (2015–2017.). Essentials of Glycobiology. Cold Spring Harbor Laboratory Press.
[22] Shi, Z.-D., Wang, H., Tarbell, J.M., Feghali-Bostwick, C., (2011). Heparan sulfate proteoglycans mediate interstitial flow mechanotransduction regulating MMP-13 expression and cell motility via FAK-ERK in 3D collagen. *PLoS ONE*, **6** (1), e15956.
[23] Banerjee, N.S., Moore, D.W., Broker, T.R., Chow, L.T., (2018). Vorinostat, a pan-HDAC inhibitor, abrogates productive HPV-18 DNA amplification. *Proc. Natl. Acad. Sci. U. S. A.*, **115** (47), E11138–E11147.
[24] Tkachyova, I., Fan, X., LamHonWah, A.-M., Fedyshyn, B., Tein, I., Mahuran, D.J., Schulze, A., Yan, C., (2016).

NDST1 preferred promoter confirmation and identification of corresponding transcriptional inhibitors as substrate reduction agents for multiple mucopolysaccharidosis disorders. *PLoS ONE*, **11** (9), e0162145.
[25] Siiskonen, H., Oikari, S., Pasonen-Seppanen, S., Rilla, K., (2015). Hyaluronan synthase 1: a mysterious enzyme with unexpected functions. *Front. Immunol.*, **6**, 43.
[26] Sun, M., Guo, S., Yao, J., Xiao, Y., Sun, R., Ma, W., Dong, Z., (2019). MicroRNA-125a suppresses cell migration, invasion, and regulates hyaluronic acid synthase 1 expression by targeting signal transducers and activators of transcription 3 in renal cell carcinoma cells. *J. Cell. Biochem.*, **120** (2), 1894–1902.
[27] Dafni, H., Israely, T., Bhujwalla, Z.M., Benjamin, L.E., Neeman, M., (2002). Overexpression of vascular endothelial growth factor 165 drives peritumor interstitial convection and induces lymphatic drain: magnetic resonance imaging, confocal microscopy, and histological tracking of triple-labeled albumin. *Cancer Res.*, **62** (22), 6731–6739.
[28] Hompland, T., Ellingsen, C., Øvrebø, K.M., Rofstad, E.K., (2012). Interstitial fluid pressure and associated lymph node metastasis revealed in tumors by dynamic contrast-enhanced MRI. *Cancer Res.*, **72** (19), 4899–4908.
[29] Munson, J.M., Shieh, A.C., (2014). Interstitial fluid flow in cancer: implications for disease progression and treatment. *Cancer Manage. Res.*, **6**, 317–328.
[30] Rutkowski, J.M., Swartz, M.A., (2007). A driving force for change: interstitial flow as a morphoregulator. *Trends Cell Biol.*, **17** (1), 44–50.
[31] Duvic, M., Vu, J., (2007). Vorinostat: a new oral histone deacetylase inhibitor approved for cutaneous T-cell lymphoma. *Expert Opin. Invest. Drugs*, **16** (7), 1111–1120.
[32] Mann, B.S., Johnson, J.R., Cohen, M.H., Justice, R., Pazdur, R., (2007). FDA approval summary: vorinostat for treatment of advanced primary cutaneous T-cell lymphoma. *Oncologist*, **12** (10), 1247–1252.
[33] Okubo, K., Isono, M., Miyai, K., Asano, T., Sato, A., (2020). Fluvastatin potentiates anticancer activity of vorinostat in renal cancer cells. *Cancer Sci.*, **111** (1), 112–126.
[34] Zibelman, M., Wong, Y.-N., Devarajan, K., Malizzia, L., Corrigan, A., Olszanski, A.J., Denlinger, C.S., Roethke, S. K., Tetzlaff, C.H., Plimack, E.R., (2015). Phase I study of the mTOR inhibitor ridaforolimus and the HDAC inhibitor vorinostat in advanced renal cell carcinoma and other solid tumors. *Invest. New Drugs*, **33** (5), 1040–1047.
[35] Pili, R., Liu, G., Chintala, S., Verheul, H., Rehman, S., Attwood, K., Lodge, M.A., Wahl, R., Martin, J.I., Miles, K. M., Paesante, S., Adelaiye, R., Godoy, A., King, S., Zwiebel, J., Carducci, M.A., (2017). Combination of the histone deacetylase inhibitor vorinostat with bevacizumab in patients with clear-cell renal cell carcinoma: a multicentre, single-arm phase I/II clinical trial. *Br. J. Cancer*, **116** (7), 874–883.
[36] Almeida, F., Gameiro, A., Correia, J., Ferreira, F., (2021). Histone Deacetylase inhibitors and microtubule inhibitors induce apoptosis in feline luminal mammary carcinoma cells. *Animals (Basel)*, **11** (2), 502.
[37] Chen, Y.-T., Chen, Y.-F., Chiu, W.-T., Liu, K.-Y., Liu, Y.-L., Chang, J.-Y., Chang, H.-C., Shen, M.-R., (2013). Microtubule-associated histone deacetylase 6 supports the calcium store sensor STIM1 in mediating malignant cell behaviors. *Cancer Res.*, **73** (14), 4500–4509.
[38] Bazou, D., Ng, M.R., Song, J.W., Chin, S.M., Maimon, N., Munn, L.L., (2016). Flow-induced HDAC1 phosphorylation and nuclear export in angiogenic sprouting. *Sci. Rep.*, **6**, 34046.
[39] Advani, A., Huang, Q., Thai, K., Advani, S.L., White, K.E., Kelly, D.J., Yuen, D.A., Connelly, K.A., Marsden, P.A., Gilbert, R.E., (2011). Long-term administration of the histone deacetylase inhibitor vorinostat attenuates renal injury in experimental diabetes through an endothelial nitric oxide synthase-dependent mechanism. *Am. J. Pathol.*, **178** (5), 2205–2214.
[40] Moran, H., Cancel, L.M., Mayer, M.A., Qazi, H., Munn, L. L., Tarbell, J.M., Tarbell, J., Vink, H., (2019). The cancer cell glycocalyx proteoglycan Glypican-1 mediates interstitial flow mechanotransduction to enhance cell migration and metastasis. *Biorheology*, **56** (2-3), 151–161.
[41] Bartosch, A.M.W., Mathews, R., Mahmoud, M.M., Cancel, L.M., Haq, Z.S., Tarbell, J.M., (2021). Heparan sulfate proteoglycan glypican-1 and PECAM-1 cooperate in shear-induced endothelial nitric oxide production. *Sci. Rep.*, **11** (1), 11386.
[42] Maxwell, C.A., McCarthy, J., Turley, E., (2008). Cell-surface and mitotic-spindle RHAMM: moonlighting or dual oncogenic functions? *J. Cell Sci.*, **121** (Pt 7), 925–932.
[43] Guan, P.-P., Yu, X., Guo, J.-J., Wang, Y., Wang, T., Li, J.-Y., Konstantopoulos, K., Wang, Z.-Y., Wang, P.u., (2015). By activating matrix metalloproteinase-7, shear stress promotes chondrosarcoma cell motility, invasion and lung colonization. *Oncotarget*, **6** (11), 9140–9159.
[44] Chi, A., Shirodkar, S.P., Escudero, D.O., Ekwenna, O.O., Yates, T.J., Ayyathurai, R., Garcia-Roig, M., Gahan, J.C., Manoharan, M., Bird, V.G., Lokeshwar, V.B., (2012). Molecular characterization of kidney cancer: association of hyaluronic acid family with histological subtypes and metastasis. *Cancer*, **118** (9), 2394–2402.
[45] Minucci, S., Pelicci, P.G., (2006). Histone deacetylase inhibitors and the promise of epigenetic (and more) treatments for cancer. *Nat. Rev. Cancer*, **6** (1), 38–51.
[46] Naito, S., von Eschenbach, A.C., Fidler, I.J., (1987). Different growth pattern and biologic behavior of human renal cell carcinoma implanted into different organs of nude mice. *J. Natl. Cancer Inst.*, **78** (2), 377–385.
[47] Zeng, Y., Ebong, E.E., Fu, B.M., Tarbell, J.M., Karamanos, N.K., (2012). The structural stability of the endothelial glycocalyx after enzymatic removal of glycosaminoglycans. *PLoS ONE*, **7** (8), e43168.